Journal of CO2 Utilization 85 (2024) 102864

Contents lists available at ScienceDirect

Journal of CO2 Utilization

journal homepage: www.elsevier.com/locate/jcou

Investigation of the kinetics of methanation of a post-coelectrolysis mixture on a Ni/CZP oxide catalyst

Audrey Waldvogel [a], Andrea Fasolini [b,c], Francesco Basile [b,c], Sebastien Thomas [a], Anne-Cecile Roger [a,*]

[a] Institut de Chimie et Procédés pour l'Energie, l'Environnement et la Santé (ICPEES, UMR CNRS 7515), 25 rue Becquerel, Strasbourg 67087, France
[b] Dipartimento di Chimica Industriale "Toso Montanari", Alma Mater Studiorum—Università di Bologna, Viale del Risorgimento 4, Bologna 40136, Italy
[c] Center for Chemical Catalysis - C3, Alma Mater Studiorum—Università di Bologna, Viale del Risorgimento 4, Bologna 40136, Italy

ARTICLE INFO

Keywords:
Post co-electrolysis mixture
Kinetic investigation
Ni/ceria-zirconia-praseodymia
Synthetic natural gas
CO_2 conversion

ABSTRACT

The use of synthetic natural gas (SNG) as a plug-and-play fuel coming from renewables can help to overcome the limitations given by the intermittency of renewable energy. A way to implement the production of SNG pass through the co-electrolysis of CO_2 to a mixture of hydrogen, carbon monoxide and carbon dioxide, steam and small amounts of methane, followed by CO and CO_2 methanation. The presence of different reactants and processes requires the comprehension and quantification of the kinetics of the reactions involved with the aim of optimizing methanation. In this work a kinetic model that considers both the direct CO_2 methanation and the indirect RWGS + CO methanation pathways has been developed over a Ni(10 %wt)/$Ce_{0.33}Zr_{0.63}Pr_{0.04}O_2$. The kinetic study made it possible to understand the influence of the reactants and products on the reactions through the calculation of reaction rates. This allowed to test, by linearization, the models found in the literature and their adjustment permitted to calculate sixteen kinetic parameters (activation energies, heats of adsorption and pre-exponential factors) present in the rate laws of methanation of CO_2, CO and the Reverse Water Gas Shift reaction. The models then made it possible to simulate the evolution of partial flow rates in an isothermal plug flow reactor and were compared to experimental data.

1. Introduction

Among the challenges that our society must face, the reduction of carbon dioxide emissions due to their impact on climate change is among the most urgent and hardest. In this framework green electricity will have a prominent role but its implementation in some fields requires the storage and release of this energy in chemical molecules, which requires to be transported and used easily [1,2].

For this reason, hydrogen has been pointed out as a promising energy carrier but technological and infrastructural barriers slow down its implementation [3,4]. Nevertheless, the well-developed natural gas network can be used to provide synthetic natural gas (SNG) coming from renewables as soon as the hydrogen infrastructure has been built. In fact, power-to-SNG with CO_2 as carbon source allows to produce quasi carbon neutral SNG while making the intrinsically intermittent renewable electricity develops and penetrates the energy supply field [5]. With the aim of producing SNG, the employment of co-electrolysers plays a significant role [6,7]. These systems are fed with water and CO_2 and produce a mixture of CO_2, CO, H_2 and small amount of CH_4 and steam using renewable electricity [8]. This mixture can be then converted into SNG by a catalytic process, called methanation at relatively low temperatures and using tailored-designed catalysts [9,10]. These are usually metallic based catalysts (Ni, Ru, Rh, Co) composed of metallic nanoparticles dispersed on an oxide (Al_2O_3, SiO_2, CeO_2, etc.). However, Ni is the preferred catalyst because of it low cost and sufficient performances [11–14]. On the support side, although alumina is among the most used ones, Ce-based oxides provide a reducible support with oxygen storage properties that can increase the catalytic activity and stability in redox reactions such as methanation [12,15–21]. The addition of Zr and Pr allows to further increase the number of oxygen vacancies and further favours the catalytic activity [17–21]. More specifically, the substitution of 5–10 at% of Ce by Pr for the oxide support of Ru- or Ni-based catalysts has been more recently shown to be highly beneficial for the reaction of CO_2 methanation [22–29]. Moreover, the catalyst activity can be highly

* Corresponding author.
E-mail addresses: audrey.waldvogel@yahoo.fr (A. Waldvogel), andrea.fasolini2@unibo.it (A. Fasolini), f.basile@unibo.it (F. Basile), sebastien.thomas@unistra.fr (S. Thomas), annececile.roger@unistra.fr (A.-C. Roger).

https://doi.org/10.1016/j.jcou.2024.102864
Received 13 March 2024; Received in revised form 18 June 2024; Accepted 29 June 2024
Available online 11 July 2024

influenced by the synthetic method employed which led us to the synthesis of an active Ni(10 %wt)/$Ce_{0.33}Zr_{0.63}Pr_{0.04}O_2$ (Ni/CZP) catalyst in previous works [16,30,31]. However, the optimization of the methanation process calls for the comprehension and quantification of the kinetics of the reactions involved. Indeed, the production of methane from post-coelectrolysis mixtures is pursued following three reactions: (i) direct CO_2 methanation (Reaction (1)); (ii) CO methanation (Reaction (2)) and (iii) reverse water gas shift (RWGS, Reaction (3)).

$CO_2 + 4\ H_2 \rightleftarrows CH_4 + 2\ H_2O\ \Delta_r H^0_{298\ K} = -165\ kJ\ mol^{-1}$ (Reaction 1)

$CO + 3\ H_2 \rightleftarrows CH_4 + H_2O\ \Delta_r H^0_{298\ K} = -206\ kJ\ mol^{-1}$ (Reaction 2)

$CO_2 + H_2 \rightleftarrows CO + H_2\ O\ \Delta_r H^0_{298\ K} = +41\ kJ\ mol^{-1}$ (Reaction 3)

Their contribution can depend on the reaction conditions and on the catalyst. For these reasons, kinetic models are used to predict catalyst performance and thus determine optimal operating conditions and control the heat of reaction. Thus, the CO and CO_2 methanation kinetics have been studied by different authors [32–37]. A detailed study of the kinetics of methanation was presented by Weatherbee and Bartholomew in 1982, using a Ni(3 %wt)/SiO_2 catalyst in the 227–327 °C temperature range and 1.4–1.7 bar pressure range [38]. The obtained methanation rate showed a moderate dependence on CO_2 partial pressures at low CO_2 partial pressures, approaching zero order at high partial pressures. The same behavior was obtained for hydrogen. Authors evidenced that methanation of CO_2 was inhibited by high CO concentrations indicating that CO_2 and CO are therefore adsorbed on the same active nickel sites. A complex mechanism of the Langmuir-Hinshelwood type was obtained that involves the dissociative adsorption of CO_2 into CO and atomic oxygen and the dissociative adsorption of H_2, followed by the breaking of the C—O bond of the adsorbed CO intermediate and the successive hydrogenation of adsorbed carbon and carbene into methane. Their equation can be simplified at low conversions and for a mixture containing only H_2 and CO_2 giving Eq. (1):

$$r_{metCO_2} = \frac{k_{metCO_2} \cdot \sqrt{P_{CO_2}} . {P_{H_2}}^{1,5}}{\left(\sqrt{P_{H_2}} + K_1 \cdot \sqrt{P_{CO_2}} + K_2 . P_{H_2} \cdot \sqrt{P_{CO_2}}\right)^2} \quad (1)$$

This first detailed mechanistic model has however been carried out for a highly diluted gas composition, very far from a possible commercial realization for an SNG process, where an almost complete conversion is expected with a methane content higher than 95 % in the product, that should fulfil the gas network purity requirements.

Xu and Froment [39] experimented the kinetics of methanation on a Ni(15 %wt)/$MgAl_2O_4$ catalyst in conditions more similar to industrial ones (300–400 °C, 10 bar). They estimated the parameters for the kinetics of methane steam reforming, CO and CO_2 methanation as well as the water gas reaction. In this case, the determining step of the reverse reaction of CO_2 methanation suggested the presence of an aldehyde type intermediate (–CHO). Again, the obtained equation could be simplified at low conversions, where the partial pressures of CO, CH_4 and H_2O are negligible for a CO_2/H_2 input mixture, leading to Eq. (2):

$$r_{metCO_2} = \frac{k_{metCO_2} . P_{CO_2} \cdot \sqrt{P_{H_2}}}{\left(1 + b_{H_2} . P_{H_2}\right)^2} \quad (2)$$

Ussa Aldana et al. [40] studied the methanation mechanism of CO_2 on a nickel catalyst based on ceria-zirconia. Contrary to the results presented above, the authors showed that H_2 dissociates on the Ni^0 sites, while CO_2 is activated on the ceria-zirconia support to form carbonate species. These carbonates can be then hydrogenated into formates by hydrogen atoms adsorbed on the Ni° sites located at the periphery of the Ni° particles, leading finally to the release of the methane by successive hydrogenation reactions. This shows how the contribution of Ce-based supports can change the reaction pathways and kinetic behavior.

Although the large amount of works on methanation kinetics that can be found, studies on Ni/CeZrPr oxides catalysts are still scarce in literature.

This study aims at developing a kinetic model considering the direct CO_2 methanation and the indirect RWGS + CO methanation paths on a Ni/CeZrPr oxide catalyst Ni(10 %wt)/$Ce_{0.33}Zr_{0.63}Pr_{0.04}O_2$ at atmospheric pressure and in the temperature range of 350–450 °C.

2. Experimental

2.1. Equipment and materials

The equipment used for the measurement of the kinetic behavior of the catalyst was divided in three parts: feeding of the gases, reaction area and analysis. The gases were sent using mass flow controllers (H_2, N_2 – internal standard for the GC analysis, CO_2, CH_4, CO, and Ar) and the gases were thoroughly mixed before the reaction zone and heated with heating bands. A micro-pump (GILSON - Model 321322350) fed liquid water to a vaporization chamber and steam mingled with the gas mixture. After the vaporization, the tubes were heated up to exclude water condensation. A tubular reactor (30 cm long and 3.0 mm inner diameter, d_t), where the powdered catalyst was placed, was heated at the desired temperature using a tubular furnace. The catalyst bed was located inside the isothermal zone of the furnace and fixed with quartz wool. The temperature was measured at the outlet of the catalytic bed using a thermocouple in contact with the bed. This temperature was considered as the reaction temperature. A cold trap was used to condense the water after the reactor while the dry gases were fed to the analysis zone composed by a micro gas chromatograph (INFICON 3000 MICRO GC) equipped with two columns: a MS5A to separate H_2, N_2, CH_4 and CO and a PPQ to separate CH_4, CO_2 and C_2H_6 that were quantified with TCD detectors. As the selectivity to C_2H_6 was always below 0.5 %, ethane has been neglected in the whole study. Each reaction condition was hold until stabilization of the conversion was obtained (ca 60 min) and an average of the 15 last minutes (4–5 points) was used as the mean value of conversion. The outlet molar flows have been calculated by two different methods to ensure the accuracy of the results: internal standard as basis or carbon balance.

2.2. Catalyst activation and stability

Experimental kinetic tests were carried out at atmospheric pressure in the range 350–450 °C using a previously optimized Ni(10 %wt)/$Ce_{0.33}Zr_{0.63}Pr_{0.04}O_2$ catalyst synthetized by coprecipitation with Na_2CO_3 (Ni/CZP).

A mass of 4.06 g of cerium nitrate hexahydrate (99.5 % ACROS Organics), 6.05 g of zirconium oxynitrate hexahydrate (99 % Sigma-Aldrich) and 0.49 g of praseodymium nitrate hexahydrate (99.9 %, Sigma-Aldrich) were dissolved in water to reach a 0.20 $mol_{cations}\ L^{-1}_{solution}$. Another solution was prepared by dissolving sodium carbonate in water (1.60 $mol_{cations}\ L^{-1}_{solution}$). The two solutions were simultaneously added dropwise to the beaker containing water at pH = 6.5, keeping the pH constant during the addition. A 3.5 h aging was then performed and the obtained solid was filtered and washed with distilled water. The solid was dried at 100 °C for 1 h and then calcined under air at 500 °C for 6 h with a ramp of 2.0 °C min^{-1}.

Ni impregnation was carried out by dissolving 2.0 g of nickel nitrate hexahydrate (98.5 %, Sigma-Aldrich) in water and stirring this solution together with the CZP oxide powder (4.0 g) for 15 min. After drying at 100 °C for 2 h, the impregnated powders were calcined at 500 °C for 6 h with a ramp of 2 °C min^{-1}. The final loading of the impregnated catalysts was 10.0 wt%Ni/CZP.

The main physico-chemical characteristics of the catalyst are the following: a specific surface area of 34 $m^2\ g^{-1}$ with a porous volume of 0.06 $cm^3\ g^{-1}$, and, after reduction, a Ni° surface of 4.3 $m^2\ g^{-1}$ corresponding to a dispersion of 7 % and a mean Ni particle size of 17 nm.

Preliminary tests were carried out to determine conditions under which the catalyst is stable at low conversions, which are selected as

they are far away from the thermodynamic equilibrium and allow to consider the catalytic bed as a differential reactor and to evidence the kinetic behavior of the catalyst. Thus, 3.0 mg of catalyst (sieved with particle diameter d_p in the 125–200 μm fraction) were diluted in 51.0 mg of SiC with the same granulometry and were reduced at 400 °C for 3 h (2 °C min^{-1}) under H_2/N_2 36/10 NmL min^{-1} flow (based on TPR results from [30]).

The catalyst stabilization procedure consisted in carrying out successive temperature stages at reaction temperatures (outlet of the catalytic bed) of 469 and 423 °C for 24 h, under a co-methanation reaction flow with $H_2/CO/CO_2$: 78/13/9 inlet molar composition at a GHSV of 1,260,000 h^{-1} at atmospheric pressure. A stable conversion was obtained in these conditions. After assessing the catalyst stability under these conditions, the kinetic tests were carried out at a maximal temperature of 469 °C.

In the case of COx co-methanation, the CO_2 conversion and the CO conversion refer to apparent conversions. As the theoretical CH_4 selectivity is equal to 100 % since it is the only C-based product apart from CO and CO_2 considered as reactants, the CH_4 selectivity was not discussed and the conversion of CO_X was thus equal to the CH_4 yield.

2.3. Diffusional limitations

The catalytic bed was prepared by diluting the catalyst in SiC for two main reasons, namely for its thermal properties and to provide higher height to the catalytic bed obtaining a plug flow reactor behavior. The plug flow assumption inside the reactor was validated theoretically by the absence of axial dispersion ($h_{bed}/d_p > 50$ [30,41]) and radial dispersion ($d_t/d_p > 8$ [42]). Pressure drops over the catalyst bed were below 0.20 bar and were then ignored [24].

The absence of external diffusional limitations in the selected configuration was demonstrated by carrying out two tests at different total flow rates (F) and catalyst masses, at constant GHSV. In particular, the tests were conducted in co-methanation conditions ($H_2/CO/CO_2$: 78/13/9 molar ratio, GHSV = 756,000 h^{-1}; 469°C and atmospheric pressure) with the following total inlet molar flowrates and catalyst masses (m) F_1 = 1.5 mmol min^{-1}, m_1 = 5.0 mg and F_2 = 3.0 mmol min^{-1}, m_2 = 10.0 mg. The granulometry range was 125–200 μm. The results showed similar methane yields (63 % vs 61 %), sufficiently far from thermodynamic limit of 79 % to confirm the absence of external diffusional limitations.

The absence of internal limitations was checked by carrying out tests at constant F and m (F_1, m_1) with other particle size diameter ranges: 25–50 μm, 50–100 μm and 100–125 μm. The results, shown in Fig. 1, highlights similar CO_2 conversions and indicates that internal diffusional limitations are not significant with particle size smaller than 200 μm.

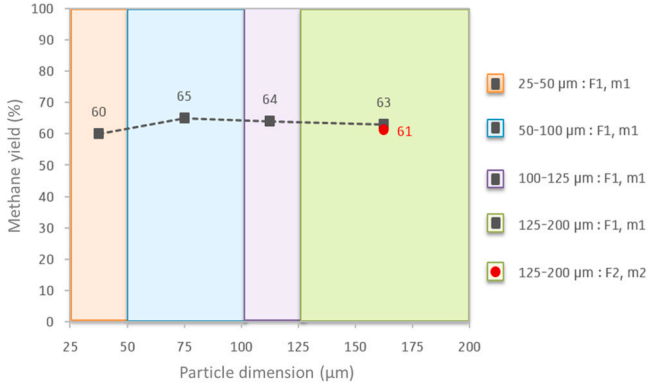

Fig. 1. Catalytic results in terms of methane yield obtained with Ni/CZP-CP (Na) at 469 °C in CO/CO_2 conditions (756,000 h^{-1}), P_{atm}, $H_2/CO/CO_2$: 78/13/9 inlet molar ratio at different catalyst dimensions or at different inlet flow (F) of catalyst mass (m).

2.4. Kinetic experiments

The Reactions (1)–(3) have been considered in this study, denoted as metCO2, metCO and RWGS, respectively. The three reverse reactions (methane reforming and water gas shift) have been considered, linked to the direct side by thermodynamics.

The methodology for the kinetic study followed two main steps.

In the first step, low conversion experiments were conducted with CO or CO_2 at the inlet. This allowed to neglect methane reforming reactions and water gas shift (except for tests with H_2O/CO at the inlet). The assumption of differential reactor allowed to identify the reaction rates laws for metCO2, metCO and RWGS, with a rough estimation of their numerical parameters. These experiments aimed at establishing the partial pressure rate dependence of each component on each reaction. This was done by varying the inlet partial pressure of one compound keeping the others constant. This was performed with compensating the varying flow with an argon flow. A maximum conversion of 20 % was tolerated to assume differential reactor and thus constant reaction rate along the reactor axis. Indeed, on the basis of low conversion, the reactants partial pressure alongside the catalyst bed was assumed to be constant, and equal to the inlet values. The reactions rates variations obtained at low conversion were then compared with those predicted by the kinetic models to select an appropriate model for each reaction

In a second step, catalytic tests were performed in conditions where higher conversion rates were reached. The reaction temperature was varied from 370 to 450 °C. The initially obtained numerical parameters were then refined using integral reactor assumption.

The variation of the kinetic constants of each reaction (k_{metCO2}, k_{metCO}, k_{RWGS}) and of the adsorption constants of the compounds (b_{H2}, b_{H2peri}, b_{CO2}, b_{CO} and b_{H2O}) with the reaction temperature makes it possible to calculate:

- a pre-exponential factor of kinetic constant A and an activation energy Ea, according to $k = A_0 e^{-Ea/RT}$.
- a pre-exponential factor of an adsorption constant b^0 and an adsorption heat Q_{ads}, according to $b_i = b_i^0.e^{Qads/RT}$.

3. Results

3.1. CO_2 methanation

The rate dependence of the CO_2 methanation on the partial pressure of the CO_2 and H_2 reactants and of the partial pressure of the CH_4 and H_2O products was established at three temperatures: 350, 375 and 400 °C. The plot of the CO_2 methanation rate (CH_4 formation rate) as a function of the partial pressures of the compounds or products makes it possible to highlight their influence on the reaction (Fig. 2).

Fig. 2a) shows that the higher the partial pressure of CO_2, the higher the rate of formation of methane. The same conclusion is drawn in the case of hydrogen for which the influence is more pronounced than for CO_2 (Fig. 2b). There is no noticeable effect of the inlet CH_4 partial pressure on the rate of its formation (Fig. 2c). On the other hand, there is an inhibiting effect of the presence of water even if outlet compositions are far from thermodynamic equilibrium (Fig. 2d).

3.2. Reverse Water Gas Shift (RWGS)

The influence of the partial pressure of the reactants CO_2 and H_2 and the influence of the partial pressure of CH_4 and H_2O were tested on the reaction rate of reverse reaction of water gas. The influence of the partial pressures was checked at the three temperatures. The results are shown in Fig. 3. It is possible to observe a quasi linear dependence of RWGS rate with CO_2 partial pressure (Fig. 3a), while the rate is clearly not

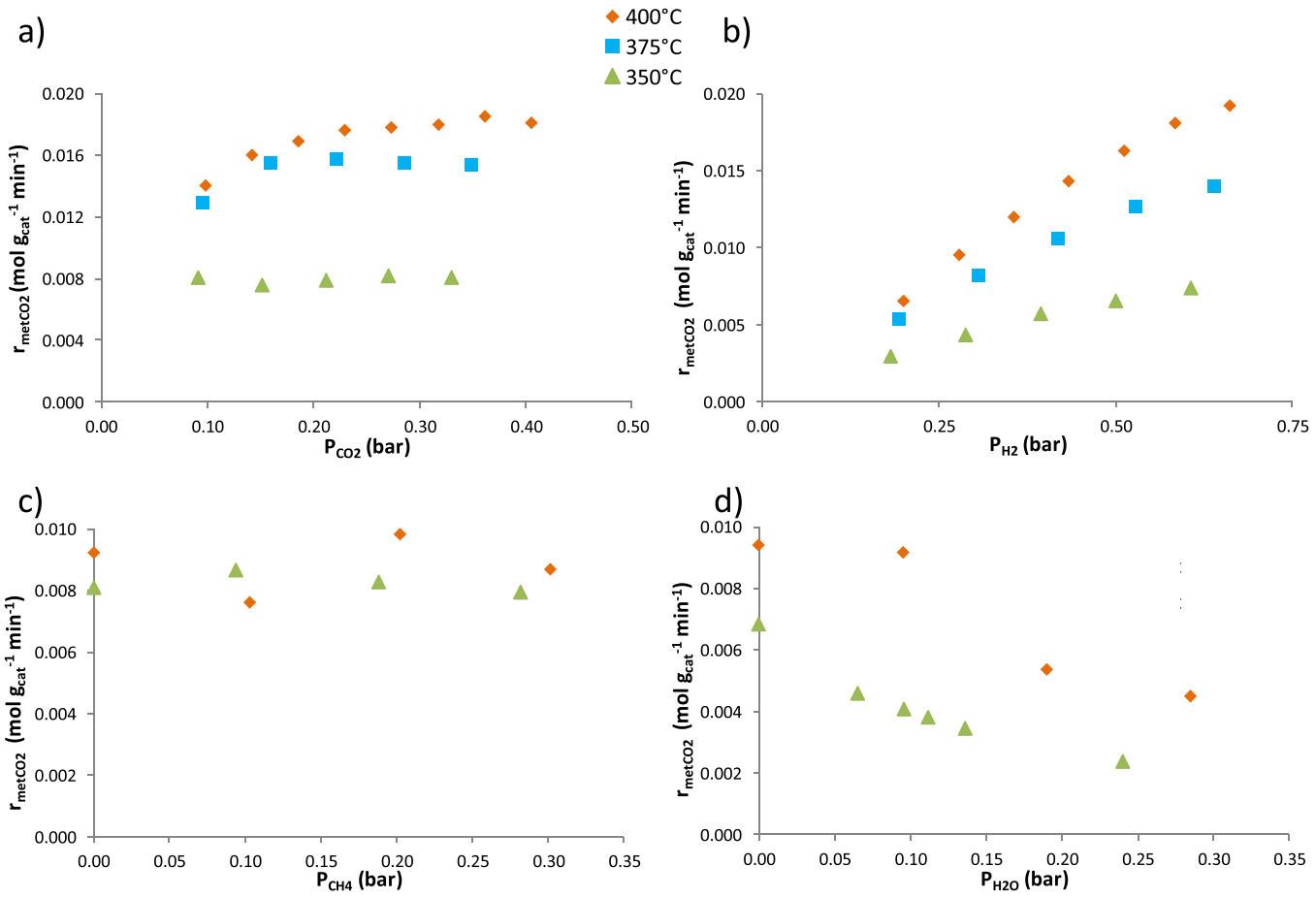

Fig. 2. Influence of the compounds pressures on the rate of methane formation in CO_2 methanation. a) influence of P_{CO2}, b) influence of P_{H2}, c) influence of P_{CH4} and d) influence of P_{H2O}.

influenced by hydrogen partial pressure (Fig. 3b). Unlike CO_2 methanation, the partial pressure of water has no effect on the RWGS reaction at low conversion, therefore far from thermodynamic limitations (Fig. 3d), so it can be postulated that the reaction sites involved are not the same involved in CO_2 activation. The presence of CH_4 does not seem to influence the RWGS reaction rate (Fig. 3c).

The influence of the partial pressure of CO on the reaction of RWGS was tested on the WGS (at 400 and 425 °C) because the latter is easier to implement from a quantitative point of view as there is no competition with the methanation reactions for a CO/H_2O mixture. Moreover, the active sites of the WGS reaction are identical to those of the RWGS and the link between the two rate expressions is given by thermodynamics. Fig. 4 shows that increasing the partial pressure of CO has a positive effect on the rate of WGS, which can be taken into account in expressing the rate of the reaction of RWGS as a function of the WGS one *via* the reaction quotient and the thermodynamic constant of the reaction.

3.3. CO methanation

Fig. 5a) and b) shows the effect of the partial pressure of the reactants (CO and H_2 respectively) on the CO methanation rate. Due to the low catalyst stability under CO/H_2 mixtures because of C deposits, only two different temperatures where tested for each partial pressure variation. It is possible to observe on Fig. 5 that the higher the partial pressure of H_2, the higher the rate of formation of methane, although this is only slightly affected by the partial pressure of CO.

4. Discussion

With the aim of defining the kinetic equations of the process, the results obtained experimentally at low conversions were fitted to the most used equations reported in the literature or their simplified version at low conversion (Eqs. (1) and (3)).

4.1. CO_2 methanation rate equation

At first, the model of Weatherbee and Bartholomew was tested by linearization of the rate law obtained for low conversions (Eq. (1)) where it is checked whether there is indeed a linear variation of $\sqrt{\sqrt{P_{CO_2}}/r_{metCO_2}}$ with $\sqrt{P_{CO_2}}$ at fixed H_2 partial pressure [38]. As shown in Fig. 6, the linearization is not verified for the lower CO_2 partial pressure tested at 350, 375 and 400 °C. This model was therefore not retained for CO_2 methanation.

An alternative model is the one proposed by Xu and Froment. Thus, Xu and Froment's model was also verified by linearizing the low-conversion rate law (Eq. (2)). This should lead to proportionality between r_{metCO2} and partial pressure of CO_2 for a constant partial pressure of H_2. This is clearly not obtained, as shown by Fig. 2a), and thus this model is not retained.

As CO_2 reaction mechanism was precisely reported by Ussa Aldana et al. [32] on the same type of catalyst Ni/CeZr oxide, the corresponding kinetic model was developed assuming surface reaction between carbonates and hydrogen adsorbed on the periphery of nickel particles as the rate determining step. When only CO_2 and H_2 are present in the feed, this assumption on the mechanism leads to Eq. (3).

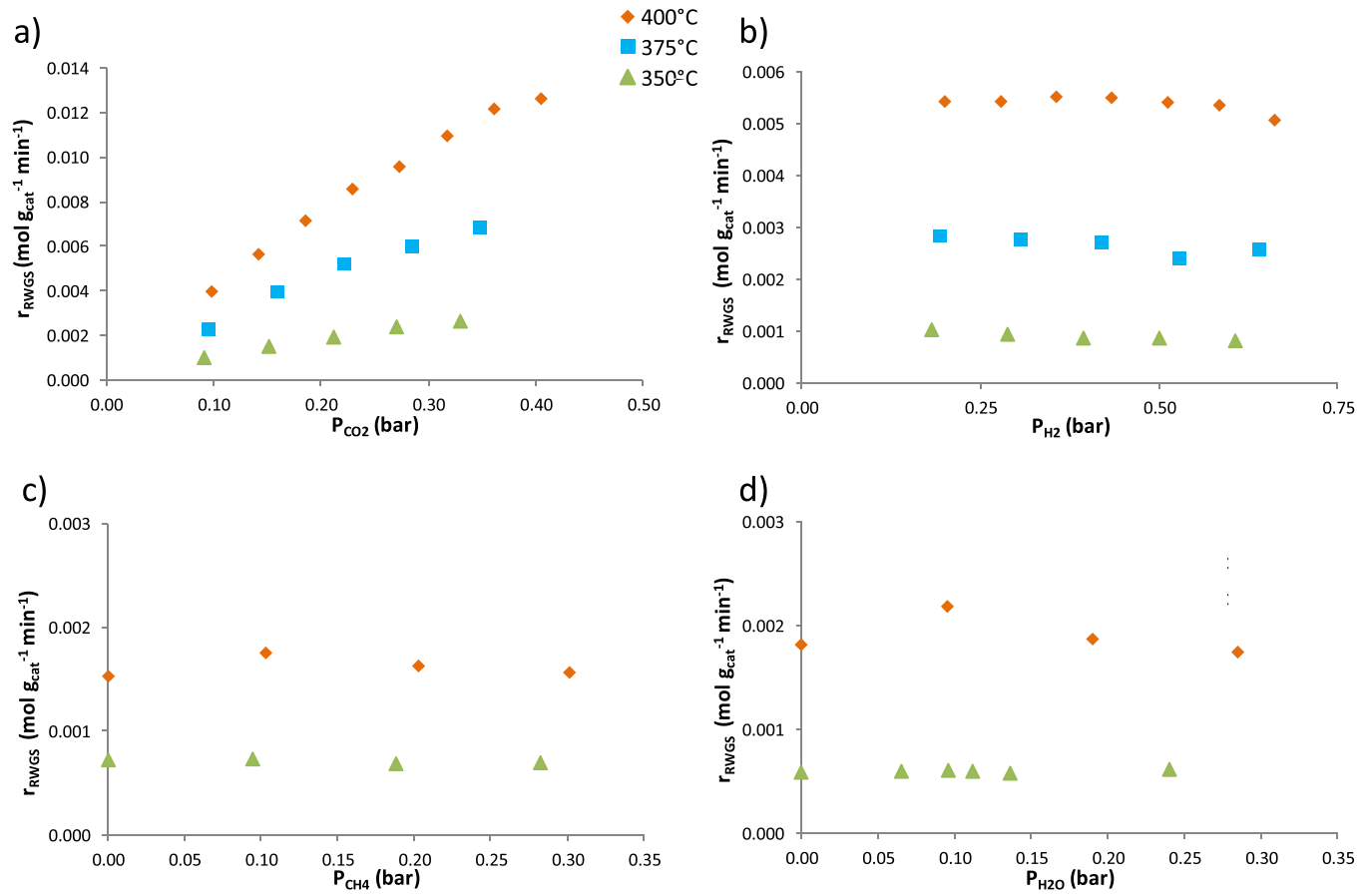

Fig. 3. Influence of the compounds pressures on the rate of reverse water gas shift reaction rate. a) influence of P_{CO2}, b) influence of P_{H2}, c) influence of P_{CH4} and d) influence of P_{H2O}.

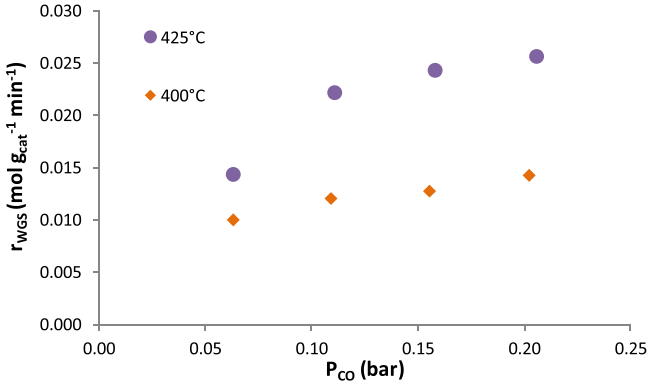

Fig. 4. Influence of the CO pressure on the water gas shift reaction rate.

$$r_{metCO_2} = \frac{k_{metCO_2}.b_{CO_2}.P_{CO_2}.b_{H_2peri}.P_{H_2}}{(1 + b_{CO_2}.P_{CO_2}).(1 + b_{H_2peri}.P_{H_2})} \quad (3)$$

Nevertheless, with CO in the feed as well as water and methane formed in significant amounts, this equation has to be adapted. Indeed, it must be considered that water can be adsorbed on ceria and CO and methane can also interact with nickel over the investigated catalysts. Actually, the effect of water was demonstrated by the results shown in Fig. 2d) where a negative influence on the reaction rate is observed in presence of water. Thus, competitive adsorption must be taken into account by the addition of the terms $b_{H2O} \times P_{H2O}$ at the denominator in the term of adsorption on ceria based support. In addition, the study of the reverse water gas reaction presented (Fig. 4) highlights the influence of the partial pressure of CO on the rate of its reverse reaction of the water gas. It is therefore possible to conclude that there is also an influence of the partial pressure of CO on the rate of methanation of CO_2, with the appearance of the term $b_{CO} \times P_{CO}$ in the denominator of the rate equation in the term of adsorption on the nickel surface. However, the addition of methane in the feed did not lead to a significant decrease in the CO_2 methanation rate (Fig. 2d) indicating that methane adsorption can be neglected. Therefore, the equation of CO_2 methanation rate takes the following final form (Eq. (4)):

$$r_{metCO_2} = \frac{k_{metCO_2}.b_{CO_2}.P_{CO_2}.b_{H_2peri}.P_{H_2}}{(1 + b_{CO_2}.P_{CO_2} + b_{H_2O}.P_{H_2O}).(1 + b_{CO}.P_{CO} + b_{H_2peri}.P_{H_2})} \quad (4)$$

The linear variation of $1/r_{metCO2}$ with $1/P_{CO2}$ at fixed P_{H2} and the linear variation of $1/r_{metCO2}$ with $1/P_{H2}$ at fixed P_{CO2} were verified on Fig. 7a) and b) respectively, attesting the possible validity of such a model for the tested catalyst.

The influence of water is verified by linearization of Eq. (4) which leads to plot $1/r_{metCO2}$ as a function of P_{H2O} at fixed P_{CO2} and P_{H2} and with small quantities of CO produced (Fig. 8). Indeed, linear variations are well observed at 350 and 400 °C, as shown in Fig. 2d), and no influence of methane partial pressure was observed.

The rate law adopted for the methanation of CO_2 is therefore Eq. (4). This equation includes a rate constant (k_{metCO2}) and 4 adsorption constants (b_{H2peri}, b_{CO2}, b_{H2O} and b_{CO}). As the presence of CO in the feed would make it impossible the individual methanation of CO and CO_2, the influence of CO on CO_2 methanation has not been directly studied. As a consequence, only b_{H2peri}, b_{CO2}, b_{H2O} parameters values were estimated from the slopes and y-intercepts of the lines shown in Figs. 7 and 8.

The values of the rate constant and the adsorption constants are then

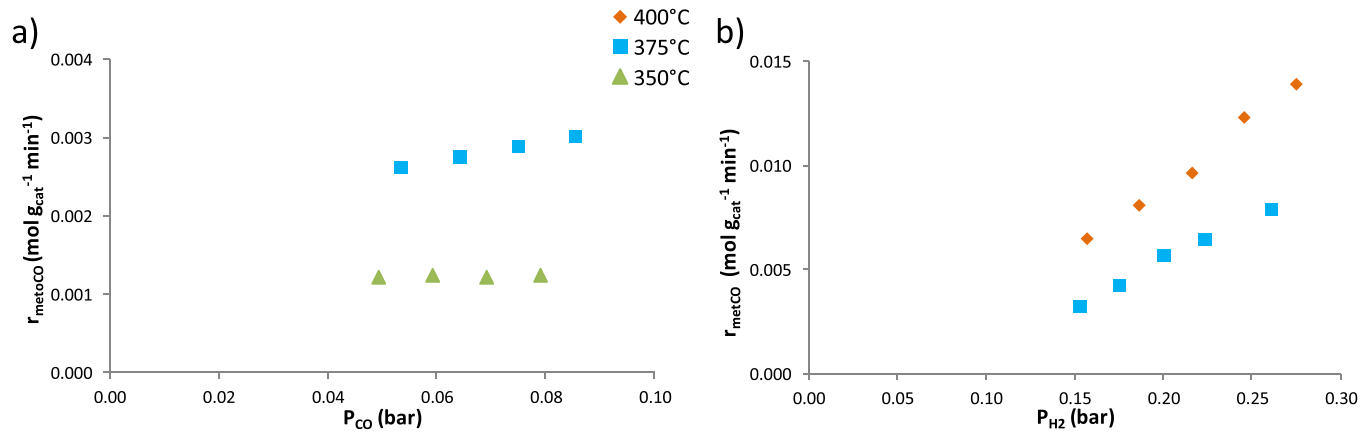

Fig. 5. Influence of reactants partial pressure on the rate of CO methanation: a) CO; b) H_2.

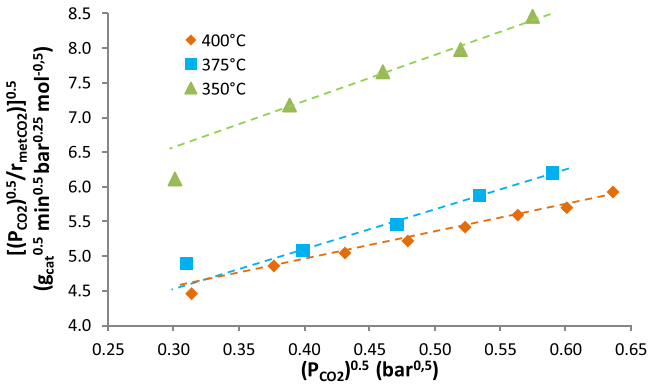

Fig. 6. Linearization of CO_2 partial pressure for the Weatherbee and Bartholomew equation in the CO_2 methanation reaction.

used to draw Fig. 9 and the resulting straight lines make it possible to estimate:

- the pre-exponential factor of the rate constant and its activation energy ($k = A_0.e^{-Ea/RT}$).
- the pre-exponential factors of the adsorption constants as well as the corresponding heats of adsorption ($b_i = b_i^0.e^{Qads/RT}$).

The variations of the parameters with the temperature are consistent. Thus, a total of eight terms were estimated (Table 1). The value obtained for hydrogen heat of adsorption on the periphery of the Ni° particles is close to those corresponding to the heat of adsorption of hydrogen on nickel surface found in the literature [43]. The heat of adsorption of CO_2 on ceria of 99.0 kJ mol^{-1} corresponds to carbonates on medium basic sites [44], which is in good agreement with the general assumption that medium basicity of the support enhances CO_2 methanation [45]. Moreover, the value obtained for water heat of adsorption on ceria is not far with values reported in the literature generally slightly higher than 50 kJ mol^{-1} [46,47].

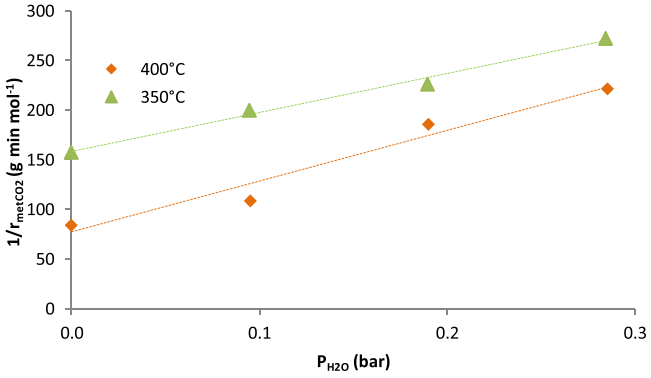

Fig. 8. Linearization of water partial pressure influence for the Ussa Aldana model of the CO_2 methanation reaction.

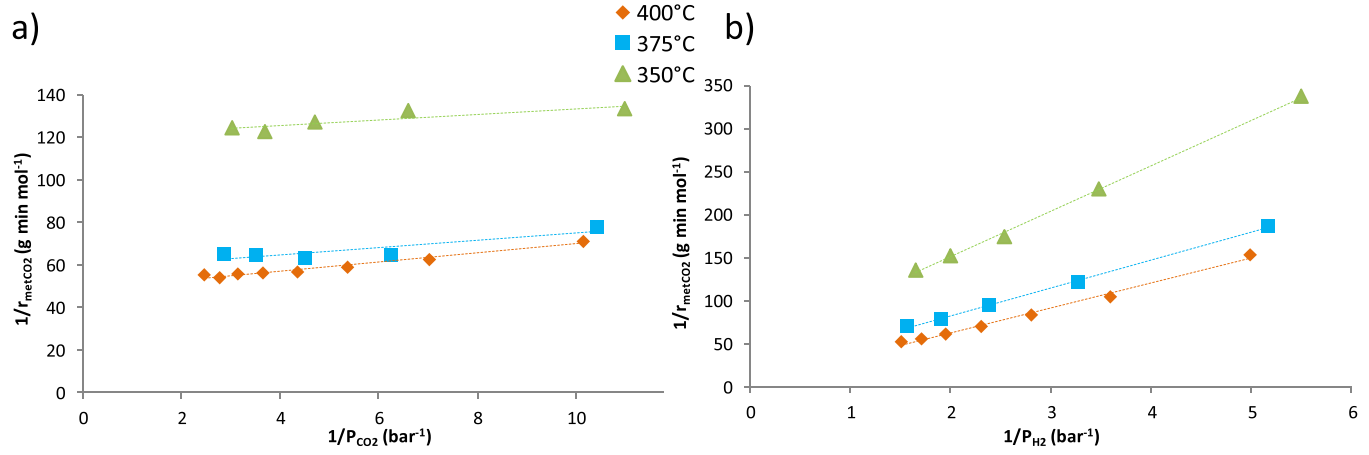

Fig. 7. Linearization of a) CO_2 and b (H_2 partial pressure influence for the Ussa Aldana model of the CO_2 methanation reaction.

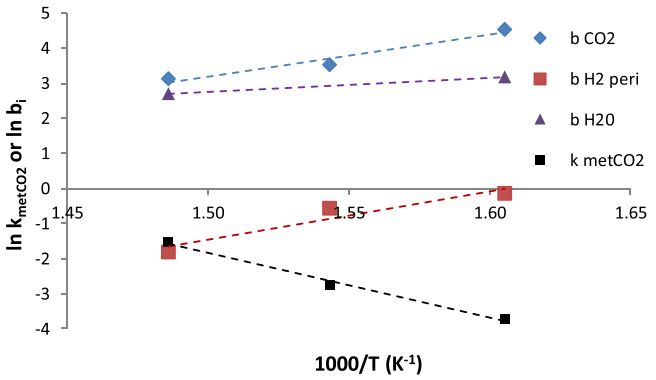

Fig. 9. Arrhenius plots for CO_2 methanation and Van't Hoff plots for b_{CO2}, b_{H2peri} and b_{H20}; k_{metCO2} in mol g^{-1} s^{-1} and b_{CO2}, b_{H2peri} and b_{H20} in bar^{-1}.

Table 1
Constants estimated from Ussa Aldana model for CO2 methanation.

$E_{a\ metCO2}$ (kJ mol^{-1})	153	A_{metCO2} (mol g^{-1} s^{-1})	$1.63.10^{11}$
$Q_{ads\ H2\ péri}$ (kJ mol^{-1})	115	$b^0_{H2\ péri}$ (bar^{-1})	$2.07.10^{-10}$
$Q_{ads\ CO2}$ (kJ mol^{-1})	99.0	b^0_{CO2} (bar^{-1})	$4.01.10^{-7}$
$Q_{ads\ H2O}$ (kJ mol^{-1})	32.4	b^0_{H2O} (bar^{-1})	$4.50.10^{-2}$

4.2. Reverse water gas shift rate equation

In addition to CO_2 methanation mechanism, in their work, Ussa Aldana et al. [40] have also described the RWGS occurring on Ni/Ceria-based catalyst. Indeed, they demonstrated that CO_2 dissociation occurs on Ni° surface which is then cleaned by adsorbed hydrogen.

This mechanism can be decomposed in the following steps, in addition to the carbonate formation on Ce^{4+} sites:

$$CO_2 + Ce^{4+} \leftrightarrow Ce^{4+}\text{-carbonate} \quad \text{(Reaction 4)}$$

$$2\ Ni + H_2 \leftrightarrow 2\ Ni\text{-}H \quad \text{(Reaction 5)}$$

$$Ni\text{-}H + Ce^{4+} \rightarrow Ni + Ce^{3+} + {}^1/_2\ H_2O \quad \text{(Reaction 6)}$$

$$CO_2 + Ce^{3+} \rightarrow CO + Ce^{4+} \quad \text{(Reaction 7)}$$

RWGS rate can be expressed as the rate of Reaction (7):

$$r_{RWGS} = k_7\ P_{CO2}\ [Ce^{3+}] \quad (5)$$

Moreover, at steady state the concentration of Ce^{3+} surface sites is constant, which implies that rates of Reactions (6) and (7) are equal. This leads to:

$$k_6\ [Ni\text{-}H]\ [Ce^{4+}] = k_7\ P_{CO2}\ [Ce^{3+}] \quad (6)$$

This allows to link $[Ce^{3+}]$ and $[Ce^{4+}]$:

$$[Ce^{4+}] = \frac{k_7 P_{CO_2} [Ce^{3+}]}{k_6 [Ni - H]} \quad (7)$$

By using thermodynamic equilibrium between neighbour pairs of Ni-H and Ni free sites as well as hydrogen partial pressure, Eq. (7) becomes:

$$[Ce^{4+}] = \frac{k_7 P_{CO_2} [Ce^{3+}]}{k_6 b_{H_2} P_{H_2}} \quad (8)$$

Balance on surface cerium sites leads to Eq. (9)

$$[Ce_{surf}] = [Ce^{3+}] + [Ce^{4+}] + [Ce^{4+}\text{-carbonate}] \quad (9)$$

By using thermodynamic equilibrium between carbonates, Ce^{4+} free sites and CO_2 partial pressure, Eq. (9) becomes:

$$[Ce_{surf}] = [Ce^{3+}]\left[1 + \frac{k_7 P_{CO_2}}{k_6 b_{H_2} P_{H_2}}(1 + b_{CO_2} P_{CO_2})\right] \quad (10)$$

By using $k_{RWGS} = k_7\ [Ce_{surf}]$ and $k_6 = k_{red}$, this finally leads to the expression of RWGS rate:

$$r_{RWGS} = \frac{k_{RWGS} k_{red} b_{H_2} P_{H_2} P_{CO_2}}{k_{red} b_{H_2} P_{H_2} + k_{RWGS} P_{CO_2} (1 + b_{CO_2} P_{CO_2})} \quad (11)$$

The rate law described in Eq. (11) was tested by plotting P_{H2}/r_{RWGS} as a function of P_{H2} at fixed P_{CO2} (Fig. 10 b). Linear relationships were indeed obtained for the three temperatures. However, negative intercepts were obtained. As the model requires positive values for this parameter, the fitting was defined as inconsistence and this model will not be retained.

The Wheeler et al. model (Eq. (12)) was then tested by linearizing the rate law obtained for low conversions [48].

$$r_{RWGS} = \frac{k_{RWGS} . b_{CO_2} . P_{CO_2} . b_{H_2} . P_{H_2}}{(1 + b_{H_2} . P_{H_2} + b_{CO_2} . P_{CO_2})^2} \quad (12)$$

It is checked whether there is indeed a linear variation of $\sqrt{P_{CO_2}/r_{RWGS}}$ with P_{CO2} at fixed H_2 partial pressure and a linear variation of $\sqrt{P_{H_2}/r_{RWGS}}$ with P_{H2} at fixed partial pressure of CO_2. A good linearization was obtained in both cases as presented in Fig. 11 a) and b). Arrhenius plots of the kinetic constant and adsorption heat also led to satisfactory linear trends (not shown). Nevertheless, calculation of the heat of adsorption of CO_2 below 10 kJ mol^{-1} (Table 2) seems not realistic as already discussed. Moreover, heat of adsorption obtained for H_2 (26.2 kJ.mol^{-1}) is very far from the value previously obtained for $H_{2\ peri}$ (115 kJ.mol^{-1}), which is, as already mentioned, in good agreement with values of the literature, and led us to reject this model.

Thus, the Xu and Froment model was tested by linearizing the rate law obtained in Eq. (13) [39].

$$r_{RWGS} = \frac{k_{RWGS} . P_{CO_2}}{(1 + b_{H_2} . P_{H_2})^2} \quad (13)$$

Here, the RWGS rate was plotted as a function of P_{CO2} at fixed P_{H2} (Fig. 12a), and the square root of the inverse of the velocity of RWGS was plotted as a function of P_{H2} at fixed P_{CO2} (Fig. 12b). A proportionality in the first case and a linear variation in the second case are well observed. As can be noticed on Fig. 3c) and d), methane and water partial pressures have no significant influence on RWGS reaction rate.

As it was mentioned previously, the partial pressure of CO influences the WGS reaction. Thus the term $b_{CO}.P_{CO}$ was introduced at the denominator of the rate equation to consider the competitive adsorption between CO and H_2 on nickel. The equation thus becomes:

$$r_{RWGS} = \frac{k_{RWGS} . P_{CO_2}}{(1 + b_{CO} . P_{CO} + b_{H_2} . P_{H_2})^2} \quad (14)$$

From the above equation, the WGS reaction rate equation, obtained by the formula $r_{WGS} = r_{RWGS} . \frac{A_{RWGS}}{K_{RWGS}}$, can be written as follows:

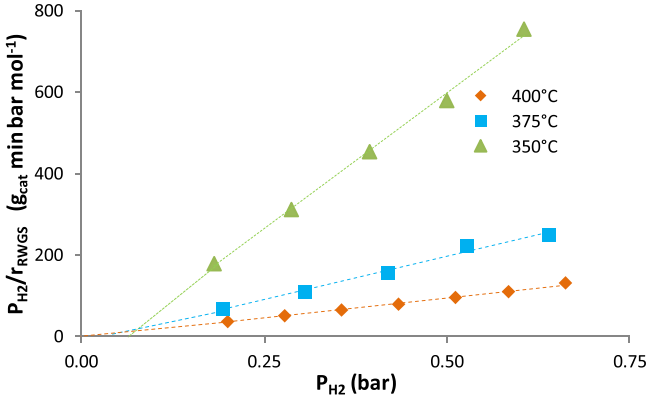

Fig. 10. Linearization of H_2 partial pressure of Eq. (11) for the reverse water as shift reaction.

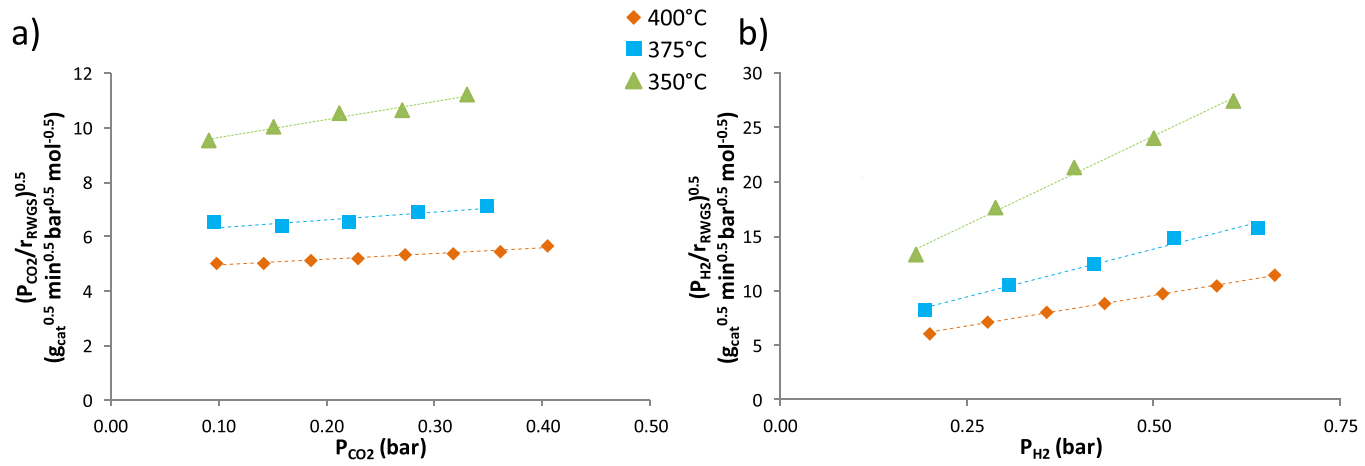

Fig. 11. Linearization of a) CO_2 and b) H_2 partial pressure of Eq. (12) for the RWGS reaction.

Table 2
Parameters associated with the model of Wheeler for RWGS.

$E_{a\ RWGS}$ (kJ mol^{-1})	164	A_{RWGS} (mol g^{-1} s^{-1})	5.05 10^{8}
$Q_{ads\ H2}$ (kJ mol^{-1})	26.2	b^{0}_{H2} (bar^{-1})	3.07 10^{-2}
$Q_{ads\ CO2}$ (kJ mol^{-1})	9.94	b^{0}_{CO2} (bar^{-1})	2.48 10^{-1}

$$r_{WGS} = \frac{k_{RWGS}.P_{CO}.P_{H_2O}}{K_{RWGS}.P_{H_2}.(1 + b_{CO}.P_{CO} + b_{H_2}.P_{H_2})^2} \quad (15)$$

As shown in Fig. 13, this last equation is verified by linearization of data from Fig. 4 and is thus used for the reverse water gas reaction equation rate.

The parameters k_{RWGS} and b_{H2} were calculated for each temperature tested for RWGS from the parameters of the trend lines of Fig. 12 whereas b_{CO} was calculated at 400 and 425 °C from the ratio slope/y-intercept of the trend lines of the linearization of WGS reaction (Fig. 13). Arrhenius and Van't Hoff plots of these parameters (Fig. 14) allow the determination of the activation energy of RWGS and the heat of adsorption of H_2 and CO on the nickel surface (Table 3), as well as the corresponding pre-exponential factors. Adsorption heats of hydrogen on nickel $Q_{ads\ H2}$ and on the periphery of nickel particles $Q_{ads\ H2\ peri}$ were found similar with 106 and 115 kJ.mol^{-1} respectively. Moreover, same order of magnitude was observed for the corresponding pre-exponential factors of b_{H2peri} and b_{H2} (Tables 1 and 3). The value of the heat of adsorption of carbon monoxide on the nickel surface $Q_{ads\ CO}$ obtained is close to the ones reported in the literature [49,50].

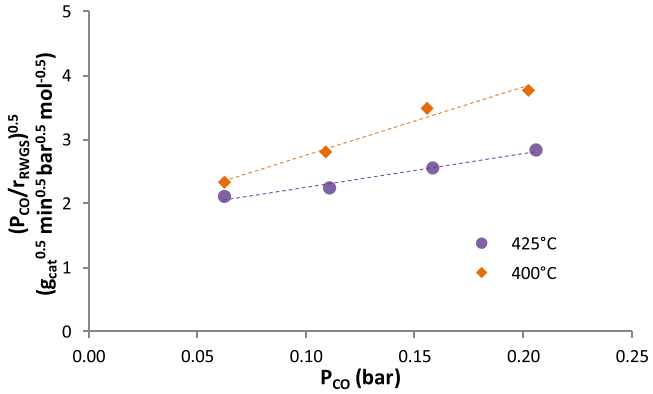

Fig. 13. Linearization CO partial pressure of Eq. (15) for the water gas shift reaction rate.

4.3. CO methanation rate equation

Finally, a plot of the results obtained with regard to CO methanation was conducted based on the kinetic model proposed by Alstrup [51], where the rate determining step is assumed to be the hydrogenation of the surface atomic carbon issued from dissociative CO adsorption. The CO methanation rate (Eq. (16)) is obtained by considering pairs of sites for H_2 adsorption and CO dissociation. It has been observed in Fig. 3d for

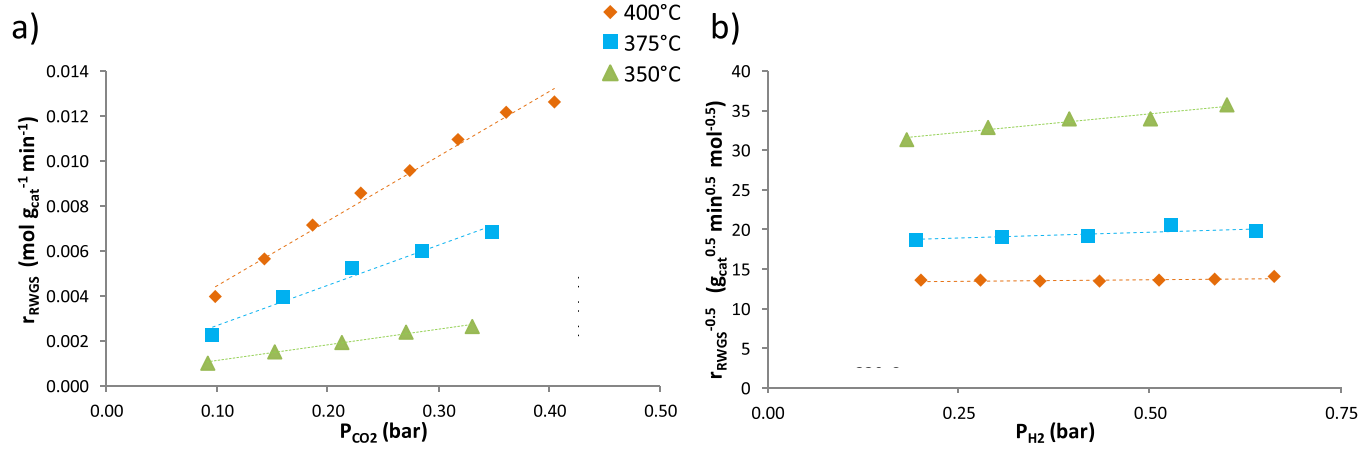

Fig. 12. Linearization of a) CO_2 and b) H_2 partial pressure of Eq. (13) for the reverse water as shift reaction.

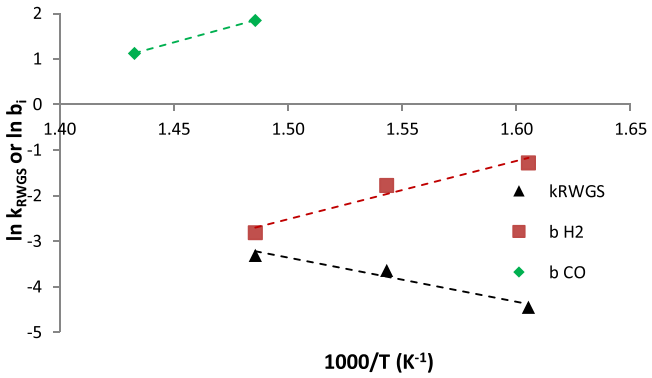

Fig. 14. Arrhenius plots for the reverse water gas shift reaction and Van't Hoff plots for b_{CO} and b_{H2}; k_{RWGS} in mol g^{-1} s^{-1} bar^{-1} and b_{CO} and b_{H2} in bar^{-1}.

RWGS that P_{H2O} does not have influence on the rate of reaction. As the same metal Ni° active sites are involved for both RWGS and CO methanation, the effect of water was also neglected for CO methanation. This is in good agreement with the model proposed by Alstrup et al. [51] which was selected in this work. This model also neglects the CHx surface concentration on Ni and thus the effect of methane on the CO methanation kinetics. The influence of the presence of CO_2 was not initially taken into account because it was previously shown that the CO_2 was mainly activated on the support and not on the metal.

$$r_{metCO} = \frac{k_{metCO}.b_{CO}.P_{CO}.b_{H_2}.P_{H_2}}{(1 + b_{CO}.P_{CO} + b_{H_2}.P_{H_2})^2} \quad (16)$$

The expression is checked by plotting $\sqrt{\frac{P_{CO}}{r_{metCO}}}$ as a function of P_{CO} (Fig. 15). A linear trend is indeed obtained for the two temperatures of 350 and 375 °C. Moreover, the quasi proportionality between r_{metCO} and P_{H2} observed in Fig. 5b) seems to indicate a lower value of $b_{H2} \times P_{H2}$ compared to $1 + b_{CO} \times P_{CO}$ in the range of the studied partial pressures. This is consistent with values of Table 3 in which b_{CO} is one order magnitude higher than b_{H2}. The rate equation is therefore validated in CO methanation.

The kinetic constant k_{metCO} and the adsorption constant b_{CO} were calculated from the slopes and the y-intercepts of the trend lines of Fig. 15 as well values of b_{H2} calculated from Table 3. The corresponding activation energy and adsorption heat were calculated from the Arrhenius laws and reported in Table 4. Values obtained for CO adsorption are consistent with the ones obtained from RWGS and average values will be taken as a starting point for parameters adjustment (Table 5).

Thus, the three kinetics equations of CO_2 methanation, RWGS and CO methanation that well fit the experimental results have been identified and are summarized below together with the 16 estimated parameters (Table 5). For each reaction, reverse reaction rate is included by the addition of the thermodynamic term in which thermodynamic constant was calculated as a function of the temperature from data from WebBook Nist.

$$r_{metCO_2} = \frac{k_{metCO_2}.b_{CO_2}.P_{CO_2}.b_{H_2peri}.P_{H_2}}{(1 + b_{CO_2}.P_{CO_2} + b_{H_2O}.P_{H_2O}).(1 + b_{CO}.P_{CO} + b_{H_2peri}.P_{H_2})} \times \left(1 - \frac{{P_{H_2O}}^2.P_{CH_4}}{K_{metCO2}.P_{CO2}.{P_{H2}}^4}\right) \quad (17)$$

Table 3
Constants calculated with the model of Xu and Froment for RWGS.

$E_{a\ RWGS}$ (kJ mol^{-1})	80.4	A_{RWGS} (mol g^{-1} s^{-1} bar^{-1})	2.00 10 3
$Q_{ads\ H2}$ (kJ mol^{-1})	106	b^0_{H2} (bar^{-1})	$4.33\ 10^{-10}$
$Q_{ads\ CO}$ (kJ mol^{-1})	114	b^0_{CO} (bar^{-1})	$8.31\ 10^{-9}$

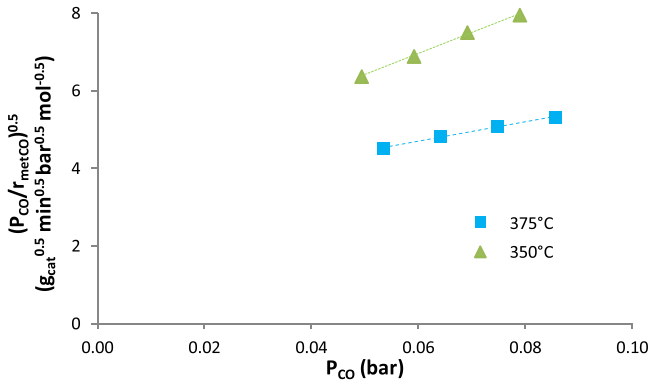

Fig. 15. Linearization of CO partial pressure for Eq. (16) of CO methanation reaction for influence of P_{CO}.

Table 4
Constants calculated for the CO methanation reaction.

Constants for CO methanation			
$E_{a\ metCO}$ (kJ mol^{-1})	173	A_{metCO} (mol g^{-1} s^{-1})	$7.16\ 10^{12}$
$Q_{ads\ CO}$ (kJ mol^{-1})	117	b^0_{CO} (bar^{-1})	$2.65\ 10^{-10}$

$$r_{RWGS} = \frac{k_{RWGS}.P_{CO_2}}{(1 + b_{CO}.P_{CO} + b_{H_2}.P_{H_2})^2} \times \left(1 - \frac{P_{H_2O}.P_{CO}}{K_{RWGS}.P_{CO2}.P_{H2}}\right) \quad (18)$$

$$r_{metCO} = \frac{k_{metCO}.b_{CO}.P_{CO}.b_{H_2}.P_{H_2}}{(1 + b_{CO}.P_{CO} + b_{H_2}.P_{H_2})^2} \times \left(1 - \frac{P_{H_2O}.P_{CH_4}}{K_{metCO}.P_{CO}.{P_{H2}}^3}\right) \quad (19)$$

5. Kinetic parameters adjustment

The results of the kinetic experiments carried out at low conversion permitted to select a kinetic model for each reaction involved and estimate their kinetic parameters. It also allowed to roughly calculate adsorption parameters of the five compounds present in the mixture. However, to validate the predictions resulting from these equations and from the 16 calculated parameters, the modeled values must be compared with experimental data obtained at higher conversions, assuming integral reactor behavior, using parity plots. In this way, it will be possible to refine the values of the 16 calculated parameters minimizing the difference between the modeled and the experimental values.

For this reason, the rate equations were applied in an isothermal plug flow reactor (PFR) model at different temperatures and GHSV. The PFR configuration allowed to introduce some approximations that simplifies the calculations of an integral reactor: (i) the reactants and products progress in successive parallel sections, neglecting axial diffusion, thus the composition varies continuously only along the longitudinal axis of the reactor; (ii) the catalytic bed was considered as one hundred successive slices corresponding to one hundred perfectly stirred reactors; (iii) the outlet partial flow of a components of each slice is considered to be the inlet flow of the next slice; (iv) the flow rate at each unit outlet is calculated from the unit inlet flow rate, the mass of catalyst in the slice and the formation and consumption rates in the slice. In this way, it was possible to estimate the partial flow rates along the PFR through the kinetics of CO_2 methanation, RWGS reaction and CO methanation and the estimated parameters at the corresponding temperature considering isobaric and isothermal reactor. The outlet molar flows obtained by the model with the estimated parameters in Table 5 were then compared to experimental values. Pre-exponential factors and activation energies were adjusted in a second step in order to minimize the root mean squared difference between the simulated partial molar outlet flows and the experimental ones. The global minimum was obtained using the Levenberg–Marquardt algorithm.

Table 5
Summary of the 16 parameters estimated without adjustment.

	Activation Energy E_a (kJ mol^{-1})	Pre-exponential factor A_0 (mol g^{-1} s^{-1})	Heat of Adsorption Q_{ads} (kJ mol^{-1})	Pre-exponential factor b_0 (bar^{-1})
CO_2 Methanation	153	1.63.10^{11}	-	-
RWGS	80.4	2.00 10^{3}	-	-
CO Methanation	173	7.16 10^{12}	-	-
CO_2 on support	-	-	99.0	4.01 10^{-7}
H_2 on peri-nickel	-	-	115	2.07 10^{-10}
H_2 on nickel	-	-	106	4.33 10^{-10}
CO on nickel	-	-	115	4.28 10^{-9}
H_2O on support	-	-	32.4	4.50 10^{-2}

The operating conditions applied are those of post co-electrolysis mixtures (feeding a $H_2/CO_2/CO/CH_4/H_2O$ mixture with a 70/8/12/5/5 molar ratio) and also of CO/CO_2 methanation (feeding a $H_2/CO_2/CO$ mixture with a 78/9/13 molar ratio). At first, a low catalyst loading (3.0 mg diluted in SiC) was used at different flow rates (100, 70 and/or 40 N mL min^{-1}) and different temperatures (450, 430, 410, 390 and/or

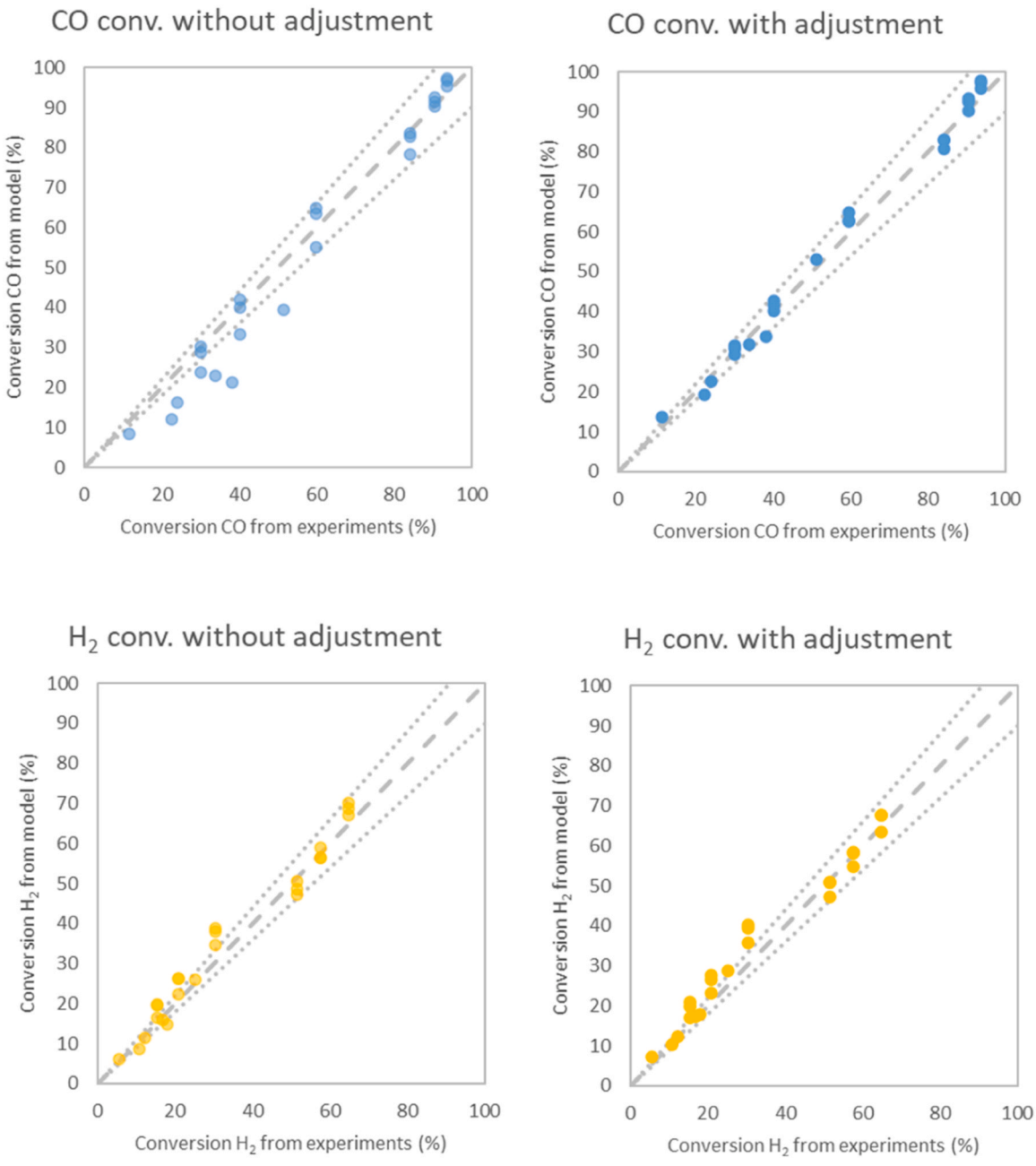

Fig. 16. Parity plots of modeled and experimental CO, CO_2 and H_2 conversion and CH_4 yield.

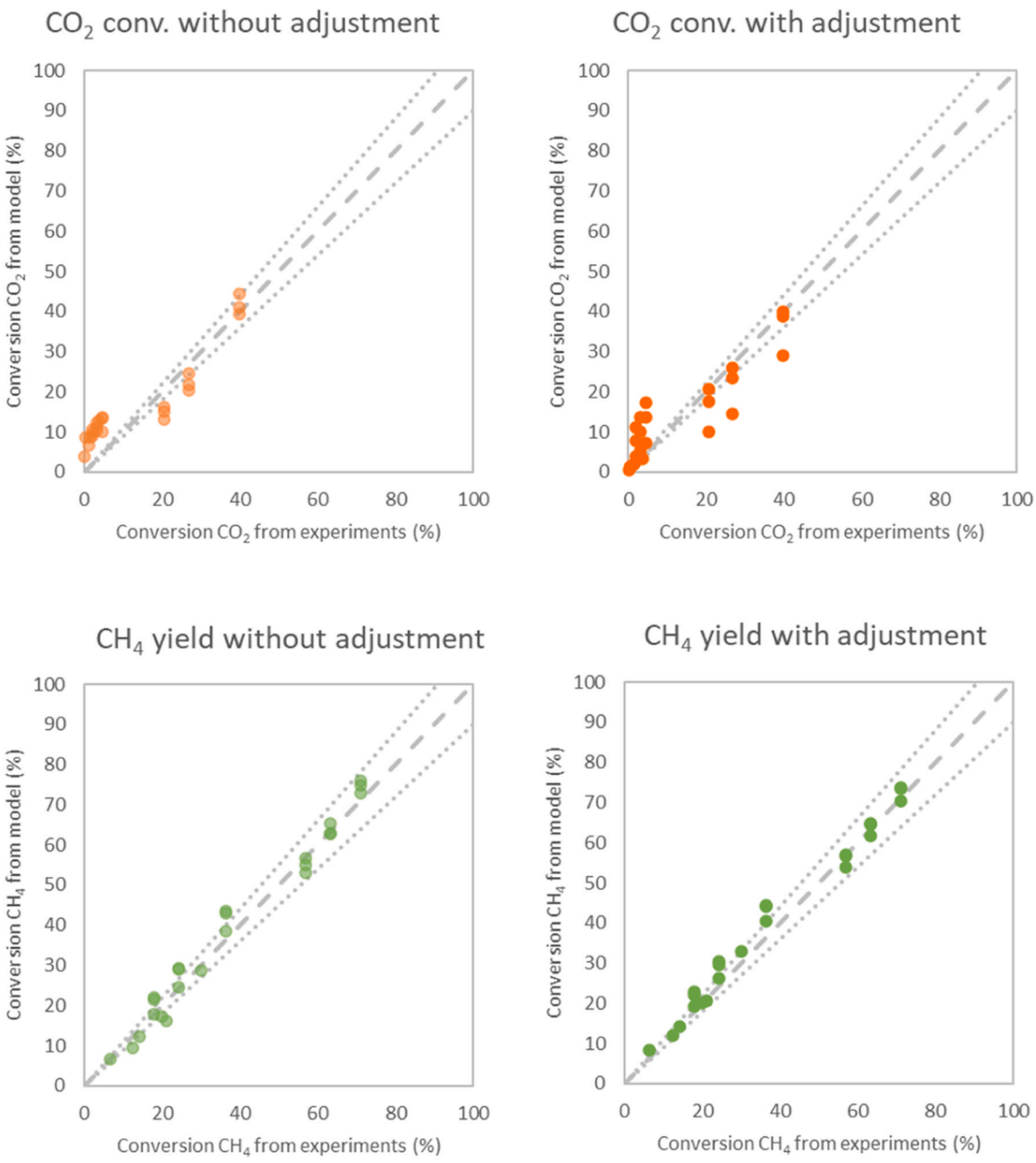

Fig. 16. (*continued*).

370 °C). Then the catalyst amount was increased (12.0 mg diluted in SiC) tested under the same conditions. In the end, a set of data from 42 different reaction conditions have been used for adjustment study.

Following the experimental tests carried out for each of the 42 different conditions, the conversions of CO, CO_2 and H_2 as well as the yield in CH_4 were obtained and were plotted over the corresponding modeled values. Fig. 16 presents the parity plots obtained, in post-co-electrolysis condition, before and after the adjustments of the kinetic parameters. An accurate model is obtained when conversion points calculated by modelling are close to the experimentally obtained conversion points. The two thin dotted lines delimit the ± 10 % deviation from the first bisector line. Without adjustment, the results obtained are quite satisfactory and the estimated methane yields have an error of ± 10 % compared to the values obtained experimentally. The parity plots obtained with adjustments of some kinetic parameters (activation energies, adsorption heats and pre-exponential factors) show a better correlation between the experimental values and the modeled values for low CO conversions (Table 6).

The activation energy of CO methanation was decreased to smooth out differences between modeled and experimental CO conversions at low temperatures. Moreover, the variation of the impact of CO_2 methanation with temperature was more consistent after adjustment. Nevertheless, the fitting is not excellent at low CO_2 conversions which could be due to competition between RWGS and methanation as well as experimental accuracy. The adjustment mainly affects the activation energy of CO_2 methanation. The parameters of the RWGS reaction were weakly tuned. The values of the activation energies obtained for the methanation of CO_2, the reaction of RWGS and the methanation of CO are 274, 79 and 176 kJ mol^{-1} respectively. It should be precised that the high value of Ea obtained for CO_2 methanation does not correspond to the apparent activation energy of the reaction but to the Ea of the rate-determining step of CO_2 methanation. When substracting the adsorption

Table 6
Final kinetic parameters estimated for the CO_2 and CO methanation and RWGS over Ni/CZP.

	Activation Energy E_a (kJ mol^{-1})	Pre-exponential factor A_0 (mol g^{-1} s^{-1})	Heat of Adsorption Q_{ads} (kJ mol^{-1})	Pre-exponential factor b_0 (bar^{-1})
CO_2 Methanation	274	3.43 10^{18}	-	-
RWGS	79.1	5.62 10^{2}	-	-
CO Methanation	176	2.77 10^{12}	-	-
CO_2	-	-	99.3	3.86 10^{-7}
$H_{2\ peri}$	-	-	115	2.07 10^{-10}
H_2	-	-	106	4.33 10^{-10}
CO	-	-	121	2.89 10^{-9}
H_2O	-	-	31.4	5.24 10^{-2}

heats of CO_2 and of H_{2peri} to 274 kJ mol^{-1}, the resulting value of 60 kJ mol^{-1} is in good agreement with values recently reported on Ni-based catalysts [52,53]. Overall, the results are very satisfactory with good agreement between the experimental values and the modeled values.

The final parameters, reported in Table 6 were able to predict with a satisfactory accuracy the experimental catalytic behavior.

6. Conclusions

In this study a kinetic model was developed based on experimental results of a Ni(10 %wt)/$Ce_{0.33}Zr_{0.63}Pr_{0.04}O_2$ catalyst considering CO_2 methanation and the indirect RWGS + CO methanation pathways. After evidencing the effect of the effect of partial pressure of reactants and products, obtained data were fitted to already reported models. Concerning CO_2 methanation, none of the established models was appropriate to describe the reaction kinetics on the Ni(10 %wt)/$Ce_{0.33}Zr_{0.63}Pr_{0.04}O_2$ catalyst. However, following the mechanistic study carried out by Ussa Aldana et al. on a Ni-CeZr oxide catalyst, a rate equation associated with the mechanism was developed by considering two sites related to the adsorption sites on the surface of the nickel and on the surface of the support. This rate equation showed good agreement with the experimental data. Regarding the reverse reaction of gas with water, it was concluded that the model of Xu and Froment was the most suitable for describing the kinetics of the reaction, while concerning the methanation of CO, the model envisaged, where the determining step is assumed to be the hydrogenation of the surface atomic carbon, showed a very good fit of the experimental data. The kinetic parameters were calculated after the linearization of the adjusted models and the establishment of Arrhenius plots and the adjusted model well fitted the experimental data.

CRediT authorship contribution statement

Audrey Waldvogel: Investigation, Data curation. **Anne-Cécile ROGER:** Writing – review & editing, Supervision, Investigation. **Sébastien Thomas:** Writing – review & editing, Supervision, Methodology, Investigation, Data curation. **Francesco Basile:** Methodology. **Andrea Fasolini:** Writing – review & editing, Writing – original draft, Investigation, Formal analysis.

Declaration of Competing Interest

On behalf of all authors, I declare that we don't have any conflict of interest related to the submitted work.

Data availability

Data will be made available on request.

Acknowledgments

Andrea Fasolini acknowledges a research contract co-funded by European Union - PON Ricerca e Innovazione 2014–2020, art. 24, comma 3, lett. a), Legge 30 dicembre 2010, n. 240 e s.m.i. e del D.M. 10 agosto 2021 n. 1062.

The authors thank ANR for funding the CHOCHO project (No. ANR-13-SEED-0002-01).

References

[1] A. Lewandowska-Bernat, U. Desideri, Appl. Energy 228 (2018) 57–67.
[2] M. Child, D. Bogdanov, C. Breyer, Energy Procedia 155 (2018) 44–60.
[3] A. Martin, M.-F. Agnoletti, E. Brangier, Int. J. Hydrog. Energy 45 (2020) 11889–11900.
[4] D. Astiaso Garcia, Int. J. Hydrog. Energy 42 (2017) 6435–6447.
[5] J. Guilera, J. Ramon Morante, T. Andreu, Energy Convers. Manag. 162 (2018) 218–224.
[6] Y. Luo, Y. Shi, W. Li, N. Cai, Energy Convers. Manag. 165 (2018) 127–136.
[7] L. Wang, M. Rao, S. Diethelm, T.-E. Lin, H. Zhang, A. Hagen, F. Maréchal, J. Van herle, Appl. Energy 250 (2019) 1432–1445.
[8] J. Herranz, A. Pătru, E. Fabbri, T.J. Schmidt, Curr. Opin. Electrochem. 23 (2020) 89–95.
[9] J. Ashok, S. Pati, P. Hongmanorom, Z. Tianxi, C. Junmei, S. Kawi, Catal. Today 356 (2020) 471–489.
[10] W.J. Lee, C. Li, H. Prajitno, J. Yoo, J. Patel, Y. Yang, S. Lim, Catal. Today 368 (2021) 2–19.
[11] J. Martínez, E. Hernández, S. Alfaro, R. López Medina, G. Valverde Aguilar, E. Albiter, M.A. Valenzuela, Catalysts 9 (2019) 24.
[12] A. Fasolini, E. Spennati, S. Ebrahim Atakoohi, M. Percivale, G. Busca, F. Basile, G. Garbarino, Catal. Today 423 (2023) 114271.
[13] P. Riani, E. Spennati, M.V. Garcia, V.S. Escribano, G. Busca, G. Garbarino, Int. J. Hydrog. Energy 48 (2023) 24976–24995.
[14] G. Busca, E. Spennati, P. Riani, G. Garbarino, Energies 16 (2023) 5304.
[15] E. Aneggi, M. Boaro, C. de Leitenburg, G. Dolcetti, A. Trovarelli, J. Alloy. Compd. 408–412 (2006) 1096–1102.
[16] F. Basile, R. Mafessanti, A. Fasolini, G. Fornasari, E. Lombardi, A. Vaccari, J. Eur. Ceram. Soc. 39 (2019) 41–52.
[17] A. Gondolini, A. Fasolini, E. Mercadelli, F. Basile, A. Sanson, Fuel Process. Technol. 213 (2021) 106658.
[18] A. Fasolini, S. Ruggieri, C. Femoni, F. Basile, Catalysts 9 (2019) 800.
[19] M. Boaro, S. Colussi, A. Trovarelli, Front. Chem. 7 (2019).
[20] J. De Maron, R. Mafessanti, P. Gramazio, E. Orfei, A. Fasolini, F. Basile, Nanomaterials 13 (2023) 53.
[21] A. Fasolini, R. Mafessanti, S. Abate, P. Gramazio, J. De Maron, G. Centi, F. Basile, Catal. Today 418 (2023) 114047.
[22] E. Poggio-Fraccari, F. Mariño, M. Laborde, G. Baronetti, Appl. Catal. A: Gen. 460–461 (2013) 15–20.
[23] M. Piumetti, T. Andana, S. Bensaid, D. Fino, N. Russo, R. Pirone, AIChE J. 63 (2017) 216–225.
[24] V.A. Sadykov, N.F. Eremeev, E.M. Sadovskaya, Y.A. Chesalov, S.N. Pavlova, V. A. Rogov, M.N. Simonov, A.S. Bobin, T.S. Glazneva, E.A. Smal, Anton I. Lukashevich, A.V. Krasnov, V.I. Avdeev, A.-C. Roger, Top. Catal. 63 (2020) 166–177.
[25] A. Auxéméry, B.B. Frias, E. Smal, K. Dziadek, G. Philippot, P. Legutko, M. Simonov, S. Thomas, A. Adamski, V. Sadykov, K. Parkhomenko, A.-C. Roger, C. Aymonier, J. Supercrit. Fluids 162 (2020) 104855.
[26] M.Y. Smirnova, A.S. Bobin, S.N. Pavlova, A.V. Ishchenko, A.V. Selivanova, V. V. Kaichev, S.V. Cherepanova, T.A. Krieger, M.V. Arapova, A.-C. Roger, A. Adamski, V.A. Sadykov, Open Chem. 15 (2017) 412–425.
[27] A.I. Tsiotsias, N.D. Charisiou, E. Harkou, S. Hafeez, G. Manos, A. Constantinou, A. G.S. Hussien, A.A. Dabbawala, V. Sebastian, S.J. Hinder, M.A. Baker, K. Polychronopoulou, M.A. Goula, Appl. Catal. B: Environ. 318 (2022) 121836.
[28] A.I. Tsiotsias, N.D. Charisiou, A. AlKhoori, S. Gaber, V. Stolojan, V. Sebastian, B. van der Linden, A. Bansode, S.J. Hinder, M.A. Baker, K. Polychronopoulou, M. A. Goula, J. Energy Chem. 71 (2022) 547–561.
[29] S.L. Rodríguez, A. Davó-Quiñonero, J. Juan-Juan, E. Bailón-García, D. Lozano-Castelló, A. Bueno-López, J. Phys. Chem. C 125 (2021) 12038–12049.
[30] A. Waldvogel, A. Fasolini, F. Basile, S. Thomas, A.-C. Roger, Energy Fuels 35 (2021) 13304–13314.

[31] M. Frey, G. Mignani, J. Jolly, A.C. Roger, Adv. Chem. Lett. 1 (3) (2013) 257–263.
[32] E.I. Koytsoumpa, S. Karellas, Renew. Sustain. Energy Rev. 94 (2018) 536–550.
[33] D. Schmider, L. Maier, O. Deutschmann, Ind. Eng. Chem. Res. 60 (2021) 5792–5805.
[34] C. Choi, A. Khuenpetch, W. Zhang, S. Yasuda, Y. Lin, H. Machida, H. Takano, K. Izumiya, Y. Kawajiri, K. Norinaga, Energy Fuels 35 (2021) 20216–20223.
[35] P. Marocco, E.A. Morosanu, E. Giglio, D. Ferrero, C. Mebrahtu, A. Lanzini, S. Abate, S. Bensaid, S. Perathoner, M. Santarelli, R. Pirone, G. Centi, Fuel 225 (2018) 230–242.
[36] L. Falbo, M. Martinelli, C.G. Visconti, L. Lietti, C. Bassano, P. Deiana, Appl. Catal. B: Environ. 225 (2018) 354–363.
[37] I. Champon, A. Bengaouer, A. Chaise, S. Thomas, A.-C. Roger, J. CO2 Util. 34 (2019) 256–265.
[38] G.D. Weatherbee, C.H. Bartholomew, J. Catal. 77 (1982) 460–472.
[39] J. Xu, G.F. Froment, AIChE J. 35 (1989) 88–96.
[40] P.A.U. Aldana, F. Ocampo, K. Kobl, B. Louis, F. Thibault-Starzyk, M. Daturi, P. Bazin, S. Thomas, A.C. Roger, Catal. Today 215 (2013) 201–207.
[41] D.E. Mears, Chem. Eng. Sci. 26 (1971) 1361–1366.
[42] C.F. Chu, K.M. Ng, AIChE J. 35 (1989) 148–158.
[43] E.K. Rideal, F. Sweett, Proc. R. Soc. Lond. Ser. A. Math. Phys. Sci. 257 (1997) 291–301.
[44] L. Atzori, M.G. Cutrufello, D. Meloni, B. Onida, D. Gazzoli, A. Ardu, R. Monaci, M. F. Sini, E. Rombi, Front. Chem. Sci. Eng. 15 (2021) 251–268.
[45] Q. Pan, J. Peng, T. Sun, S. Wang, S. Wang, Catal. Commun. 45 (2014) 74–78.
[46] D. Kaya, D. Singh, S. Kincal, D. Uner, Catal. Today 323 (2019) 141–147.
[47] S. Fuente, M.M. Branda, F. Illas, Theor. Chem. Acc. 131 (2012) 1190.
[48] C. Wheeler, A. Jhalani, E.J. Klein, S. Tummala, L.D. Schmidt, J. Catal. 223 (2004) 191–199.
[49] S. Skurnik, M. Steinberg, Ind. Eng. Chem. Fund. 6 (1967) 459–460.
[50] Z. Oda, Bull. Chem. Soc. Jpn. 28 (1955) 285–290.
[51] I. Alstrup, J. Catal. 151 (1995) 216–225.
[52] G. Garbarino, C. Wang, T. Cavattoni, E. Finocchio, P. Riani, M. Flytzani-Stephanopoulos, G. Busca, Appl. Catal. B: Environ. 248 (2019) 286–297.
[53] D. Han, W. Cho, Y. Baek, Catalysts 12 (2022) 1054–1072.